ARTICLES

Resonant Raman scattering in potassium and chlorine K_β x-ray emission from KCl

K. E. Miyano
Department of Physics, Brooklyn College, Brooklyn, New York 11210

Y. Ma
Department of Physics, University of Washington, Seattle, Washington 98195
and Pacific Northwest Laboratory, Richland, Washington 99352

S. H. Southworth and P. L. Cowan
Physics Division, Argonne National Laboratory, Argonne, Illinois 60439

B. A. Karlin
Brookhaven National Laboratory, Upton, New York 11973
(Received 21 February 1996)

We have measured the potassium K_β and chlorine K_β resonant Raman x-ray scattering from KCl. Strong K-shell absorption peaks are directly reflected in the resonant Raman spectra. The emission spectra are qualitatively evaluated in terms of the associated absorption spectra, based on a simple single-electron model of the scattering process. This model affords direct interpretation of the energy, line shape, and intensity variations of the emission spectra. In the resonant Raman regime, energy offsets between the data and the model predictions are attributed to binding energy differences between intermediate and final state excitons; thus these offsets indicate that the associated peaks in the absorption spectra are excitonic in nature. [S0163-1829(96)00341-4]

I. INTRODUCTION

Alkali halides such as KCl are model ionic compounds in which the constituent ions have closed shells and narrow valence bands. They have traditionally been of interest with respect to x-ray-absorption and emission phenomena.[1–8] There are also many recent studies of x-ray emission excited with tunable x rays near core-ionization thresholds. One such threshold phenomenon is resonant Raman x-ray scattering, in which inelastic x-ray scattering by a core or valence electron is enhanced near the excitation threshold of a deeper core electron: this enhancement occurs at scattered x-ray energies near the characteristic x-ray fluorescence. This form of scattering was first observed by Sparks[9] and was further clarified using tunable synchrotron-radiation by Eisenberger, Platzman, and Winick.[10] Since then, numerous experimental observations have been reported, for excitation to both continuum final states[11–13] and combinations of excitonic and continuum[14–19] final states. Meanwhile resonant Raman x-ray scattering has been described theoretically, based on the Kramers-Heisenberg formalism.[20,21]

Many resonant Raman studies at K-absorption thresholds have focussed on K_α emission. However, for potassium and chlorine the $2p$ spin-orbit splitting in K_α emission, on the order of 2 eV, is disadvantageous for the present study; until the two components are separated during data analysis, lineshape changes near threshold are obscured. We concentrate instead on K_β emission from both the potassium and the chlorine. Here the inelastic scattering by shallow $3p$ electrons evolves into K_β fluorescence at the $1s$ threshold. Core-to-*valence* emission exhibits special characteristics. For excitation energies just above threshold, spectra are excitation-energy dependent and spatially anisotropic due to coherence between the absorption and emission processes and consequent momentum-conservation restrictions.[22,23] In KCl the potassium and chlorine $3p$ energy bands exhibit little dispersion, and such effects are not resolved. As discussed below, one can also interpret core-to-*valence* emission in the resonant Raman regime in terms of binding-energy differences between an intermediate-state core exciton and a final-state valence exciton.[24] At threshold the core-valence emission energy lies close to the excitation energy, and hence the emission spectrum and elastic-scattering peak can simultaneously be recorded with our spectrometer. This automatic calibration of the incident photon energy is crucial: near-threshold spectra are sensitive to the exact value of this energy.

II. EXPERIMENT

Measurements were conducted at Beamline X24A of the National Synchrotron Light Source.[25] Si(111) monochromator crystals were used to select the incident photon energies; the intrinsic resolution of these crystals is 0.4 eV at 2.8 keV (chlorine K edge) and 0.6 eV at 3.6 keV (potassium K edge).[25] The secondary monochromator, that is, the x-ray-emission spectrometer,[26] employed a curved Si(111) crystal and a position-sensitive detector, allowing for simultaneous collection of an entire K emission spectrum along with the

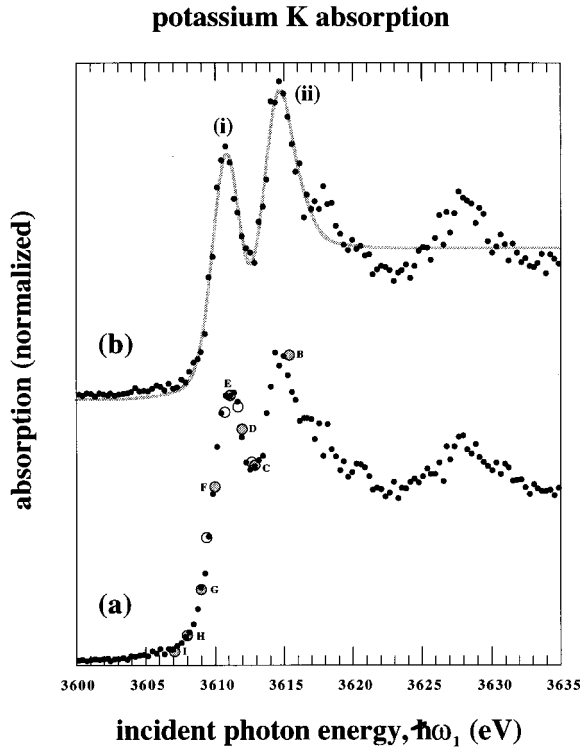

FIG. 1. Potassium fluorescence-yield spectra taken at the potassium K edge are plotted. In (a) the spectra were taken with K_α-fluorescence detection (small black points) and K_β-fluorescence detection (large gray and white circles), using a 45° angle of incidence and a 45° angle of fluorescence emission. The gray circles signify excitation energies at which K emission spectra are plotted in Fig. 2. In (b) the spectrum was taken with K_α-fluorescence detection, using near-normal incidence and grazing emission, while the solid gray line represents a model fit.

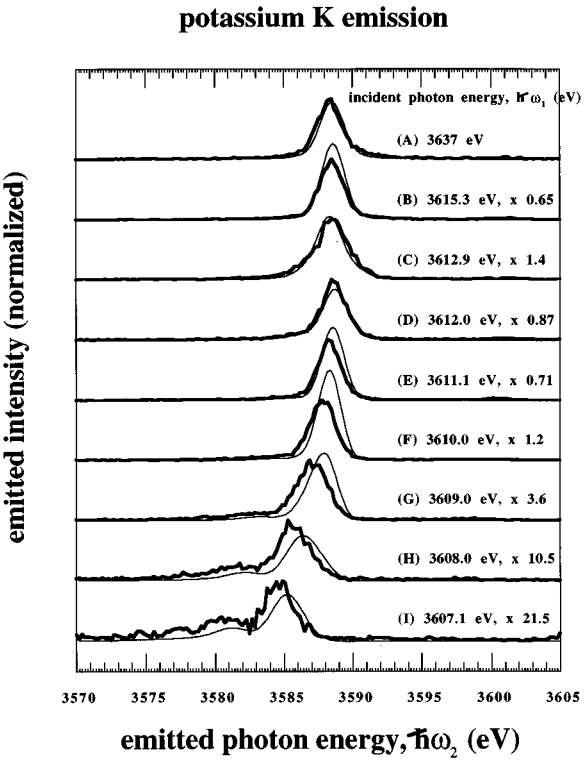

FIG. 2. Potassium K_β emission spectra (heavy lines) are plotted for different incident photon energies. The scaling factor is the number by which each flux-normalized spectrum was multiplied to match its peak height with that of spectrum (A). Absorption-based spectra constructed from Eq. (4) (thin lines) are superimposed for comparison, with the same relative scaling factors as the data.

elastic-scattering peak. The elastic-scattering peak was used initially to calibrate the full range of spectrometer energies relative to the beamline monochromator energies. The intrinsic resolution of the emission-spectrometer crystals is 0.36 eV at 2.8 keV (chlorine K_β) and 0.44 eV at 3.6 keV (potassium K_β). The widths of the elastic-scattering peaks were observed to be up to two times higher than the ideal combined resolution of the monochromator and spectrometer crystals.

Centimeter-sized samples of KCl were cleaved and placed in the sample chamber. Long exposure to the synchrotron beam led to the formation of color centers. We were careful to look for influence of this defect formation in the various spectra, and the beam spot was frequently moved on the samples. No influence of defects was observed in this experiment.

III. RESULTS

A. Potassium *K* x-ray absorption and emission

Figure 1(a) shows fluorescence-yield spectra at the potassium K edge measured with K_α and K_β fluorescence emitted 45° from the surface normal. Figure 1(b) shows yield spectra measured with K_α fluorescence emitted at glancing angles. In the glancing emission measurement the sampling depth was always less than the penetration depth of the incident x rays; the spectrum is sharp and accurately represents absorption per volume. The spectrum in Fig. 1(b) is similar to transmission spectra taken from thin films[1] and will herein be interpreted as potassium K absorption spectra.

Potassium K_β emission spectra were taken at the incident energies, $\hbar\omega_1$, for which white and gray circles appear in Fig. 1(a). In fact, the K_β-fluorescence-yield spectrum was obtained by individually integrating the areas of the flux-normalized emission spectra. In Fig. 2, some of these emission spectra are plotted, normalized to equal peak height. At the highest $\hbar\omega_1$, about 25 eV above the absorption threshold, the emission spectrum agrees with those published previously:[2,3] a single peak represents the potassium $1s$-$3p$ transition. The so-called $K_{\beta V}$ feature, representing a potassium-$1s$–chlorine-$3p$ cross transition,[3] also appears in these spectra although it is not discernable at the intensity scale of Fig. 2. As $\hbar\omega_1$ is lowered below threshold, the main emission peak shifts to lower emitted energy, $\hbar\omega_2$, and an additional lower-energy peak appears. In Fig. 3, the $K_{\beta V}$ feature is shown with a magnified intensity scale for several $\hbar\omega_1$ values; as $\hbar\omega_1$ is lowered below threshold, this feature also shifts down in $\hbar\omega_2$. In Fig. 4, the centroid energies of the main emission peak, the low-energy peak, and the $K_{\beta V}$ peak, determined using a curve-fitting routine, are plotted as a function of $\hbar\omega_1$.

B. Chlorine *K* x-ray absorption and emission

Figures 5 and 6 show chlorine fluorescence-yield and K_β emission spectra. The yield spectrum taken at glancing emis-

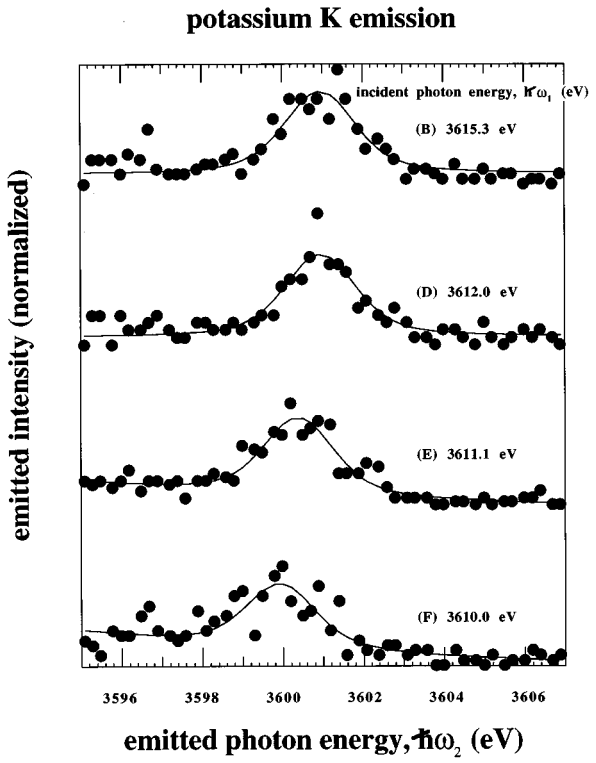

FIG. 3. The weak potassium $K_{\beta V}$ emission feature is plotted for several incident photon energies. The intensities are scaled by the same factors as in Fig. 2. Curve fits used to estimate the centroid energies of these spectra are also plotted.

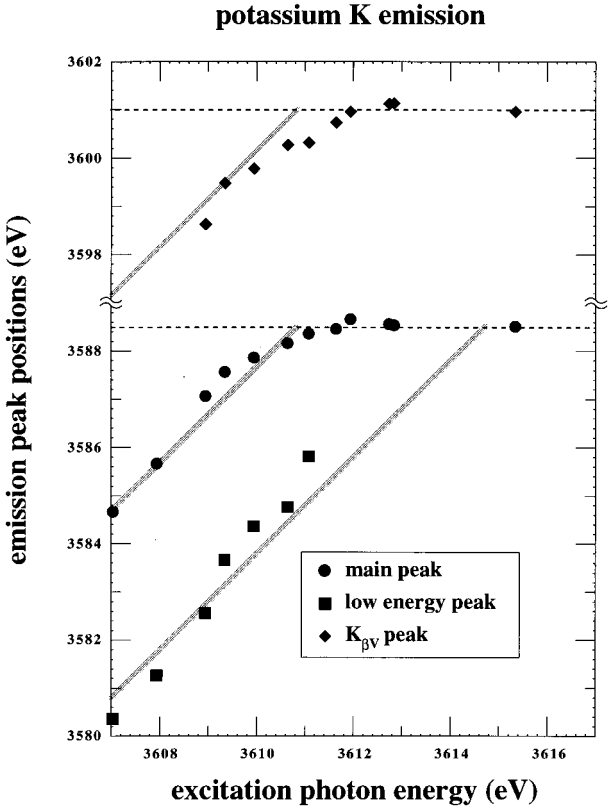

FIG. 4. Centroid energies of the measured potassium K emission peaks are plotted versus excitation energy. The resonant Raman emission energies predicted from energy conservation considerations [Eq. (1)] are also plotted as solid gray lines. The dashed lines mark the centroid energies of the main and $K_{\beta V}$ emission features for excitation energies above threshold.

sion is again sharper than those taken at 45° emission, and this will be interpreted as the chlorine K absorption spectrum. The first two peaks in the absorption spectrum are broader and their energy separation is somewhat greater than in the potassium case. The chlorine K emission spectrum taken at $\hbar\omega_1 = 2853.9$ eV [Fig. 6 (A)] has a high-energy shoulder due to emission involving a multiple-hole initial state;[3] in the other emission spectra the excitation energy is sufficiently low that this satellite is suppressed.[7] At the higher $\hbar\omega_1$, the emission spectra agree with those published previously.[2,3,7] Below threshold the chlorine K emission spectra shift to lower $\hbar\omega_2$, and at the lowest values of $\hbar\omega_1$ a shoulder appears on the low-energy side. In Fig. 7, the centroid energies of the main emission peak and the shoulder are plotted as a function of $\hbar\omega_1$.

IV. DISCUSSION

A. Energy conservation

Each resonant Raman emission feature corresponds to a certain feature in the associated absorption threshold. One can predict, based on energy conservation, the centroid energy for the Raman feature corresponding to a given absorption feature:

$$\hbar\omega_2 = E_{KM} - (E_{(n)} - \hbar\omega_1). \tag{1}$$

E_{KM} is the post-threshold K_β fluorescence energy, seen in Figs. 2 and 6 to be 3588.5 eV and 2814.7 eV for potassium and chlorine, respectively. E_{KM} for the potassium $K_{\beta V}$ feature is 3601.0 eV. $E_{(n)}$ is the energy of a feature (n) in the absorption threshold. Peaks (i) and (ii) in the potassium K absorption of Fig. 1 have $E_{(\mathrm{i})} = 3610.8$ eV and $E_{(\mathrm{ii})} = 3614.7$ eV, and the corresponding emission energies predicted by Eq. (1) are plotted in Fig. 4. In the chlorine K absorption of Fig. 5, $E_{(\mathrm{i})} = 2824.6$ eV, and the second set of features is grouped at $E_{(\mathrm{ii})} = 2829.5$ eV. Equation (1) is correspondingly plotted in Fig. 7. In Figs. 4 and 7, Eq. (1) is seen to explain the emission peak positions measured in the resonant Raman regime. In this regime of both the potassium and chlorine emission data, the main peaks are associated with absorption peaks (i), while the low-energy shoulders are associated with absorption peaks (ii). The potassium $K_{\beta V}$ Raman feature is associated with absorption peak (i), while a shoulder associated with peak (ii) could not be resolved.

B. Kramers-Heisenberg equation

A theoretical description of resonant Raman scattering[20,21] begins with the Kramers-Heisenberg equation for the differential transition cross section. Near the core excitation threshold the cross section is dominated by the resonant term, which in the dipole approximation, may be written as

$$\frac{d^2\sigma}{d\omega_2 d\Omega} = \frac{r_e^2}{m_e^2}\frac{\omega_2}{\omega_1}\left|\sum_I \frac{\langle B|\mathbf{p}\cdot\boldsymbol{\epsilon}_2|I\rangle\langle I|\mathbf{p}\cdot\boldsymbol{\epsilon}_1|A\rangle}{E_A + \hbar\omega_1 - E_I - i\Gamma_I/2}\right|^2 \times \delta(E_B + \hbar\omega_2 - E_A - \hbar\omega_1). \tag{2}$$

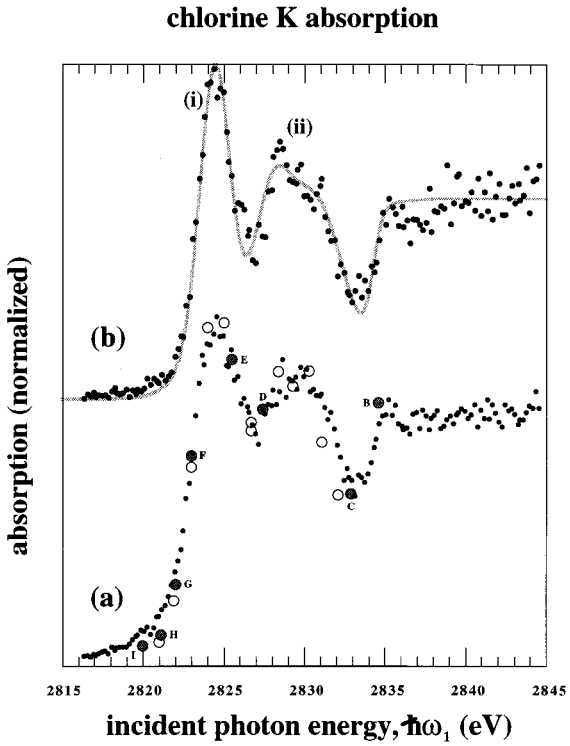

FIG. 5. Chlorine fluorescence-yield spectra taken at the chlorine K edge are plotted. In (a) the spectra were taken with K_α-fluorescence detection (small black points) and K_β-fluorescence detection (large gray and white circles), using a 45° angle of incidence and a 45° angle of fluorescence emission. In (b) the spectrum was taken with K_α-fluorescence detection, using near-normal incidence and grazing emission, while the solid gray line represents a model fit.

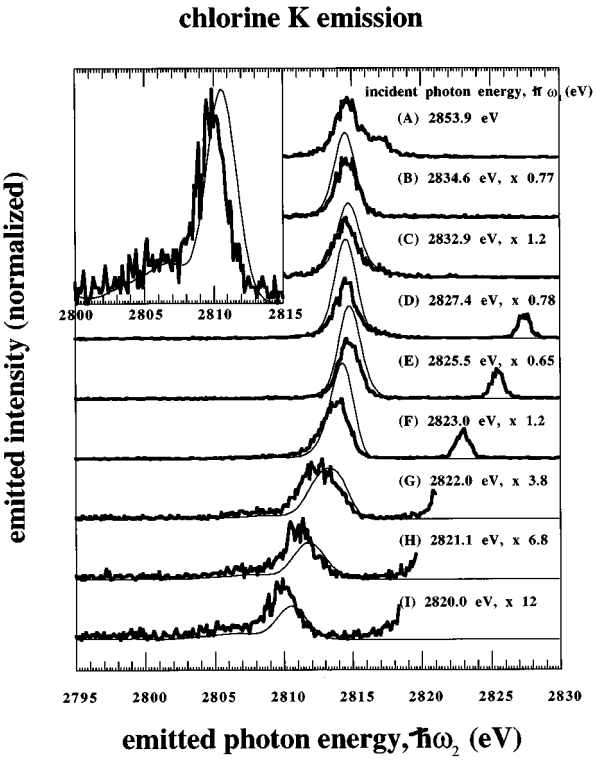

FIG. 6. Chlorine K_β emission spectra-(heavy lines) are plotted for different incident photon energies. The spectra are normalized to equal peak height, with the intensity scaling factor indicated. In spectra (G), (H), and (I), the elastic-scattering peak is more intense than the emission features and has been truncated. Absorption-based spectra constructed from Eq. (4) (thin lines) are superimposed for comparison, with the same relative scaling factors as the data. In order to accentuate the low-energy shoulder, the measured and constructed spectra for the lowest incident photon energy, 2820.0 eV, are replotted in the inset with equal peak heights.

Here r_e is the classical electron-scattering radius, and m_e is the electron rest mass; ω_1 and $\boldsymbol{\epsilon}_1$ are the frequency and polarization vector of the incident photon, while ω_2 and $\boldsymbol{\epsilon}_2$ are those for the emitted (scattered) photon; A, I, and B represent the initial, intermediate, and final states of the scattering process, and E_A, E_I, and E_B are their energies; and Γ_I is the lifetime width of the intermediate state. The summation ranges over the intermediate states; from a one-electron viewpoint it is the energy, ε, of the initially excited electron that varies for different I. These intermediate states include both excitons (negative ε) and states with the excited electron in the continuum (positive ε). The δ function expresses conservation of energy. Rewriting the denominator of Eq. (2) based on this conservation yields

$$\frac{d^2\sigma}{d\omega_2 d\Omega} = \frac{r_e^2}{m_e^2}\frac{\omega_2}{\omega_1}\left|\sum_{\varepsilon}\frac{\langle B|\mathbf{p}\cdot\boldsymbol{\epsilon}_2|I\rangle\langle I|\mathbf{p}\cdot\boldsymbol{\epsilon}_1|A\rangle}{\hbar\omega_2-(E_I-E_B)-i\Gamma_I/2}\right|^2 \times\delta(E_B+\hbar\omega_2-E_A-\hbar\omega_1). \tag{3}$$

C. Interpretation of emission spectra based on the associated absorption spectrum

Various authors[11,16,17] have described an interpretation of x-ray emission spectra in the threshold regime in terms of the associated absorption spectrum. In the context of a single-electron-excitation model, this interpretation is based on the assumption of *ε-independent emission*, meaning that the state of the initially excited electron does not influence the transition between states I and B and that the energy ε is the same in the intermediate and final states. This assumption is readily acceptable for electrons excited to continuum states, but even if the electron is excited to an excitonic level, it is presumed to only be a *spectator* to the I-B transition. Then in Eq. (3), Γ_I, (E_I-E_B), and the matrix element $\langle B|\mathbf{p}\cdot\boldsymbol{\epsilon}_2|I\rangle$ are independent of ε and can be taken outside of the summation. Dropping terms that vary slowly with ω_2 and adapting the equation specifically to M-electron scattering at the K threshold,

$$\frac{d^2\sigma}{d\omega_2 d\Omega} \propto L_K(\hbar\omega_2-E_{KM})\cdot\mu^*(\hbar\omega_1-\hbar\omega_2+E_{KM}), \tag{4}$$

where $L_K(\hbar\omega_2-E_{KM})=[(\hbar\omega_2-E_{KM})^2+\Gamma_K^2/4]^{-1}$, and μ^* is the excitation cross section, that is, the absorption spectrum with the K-hole broadening and beamline-monochromator broadening removed. Figure 8 shows that for a specific excitation energy, $\hbar\omega_1$, the product $L_K(E-\hbar\omega_1)\cdot\mu^*(E)$ represents the probability of excitation to an intermediate state of nominal energy E. Under the ε-independent-emission assumption this probability distribu-

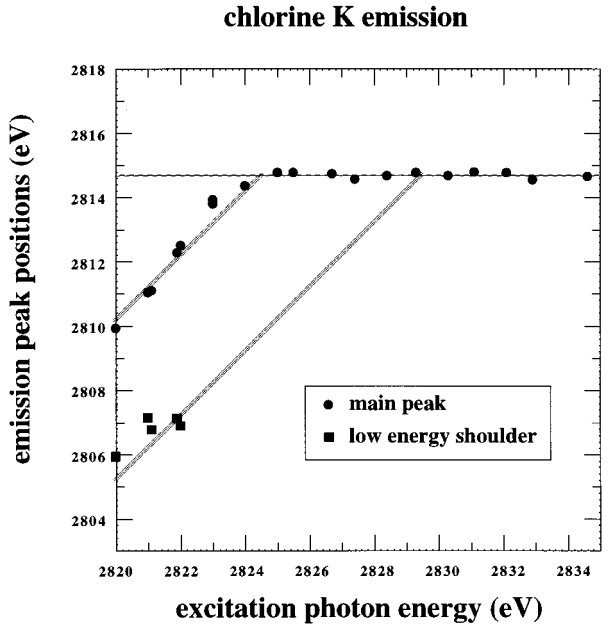

FIG. 7. Centroid energies of the measured chlorine K emission peaks are plotted vs excitation energy. The resonant Raman emission energies predicted from energy conservation considerations [Eq. (1)] are also plotted, as solid gray lines. The dashed line marks the centroid energy of the main emission peak for excitation energies above threshold.

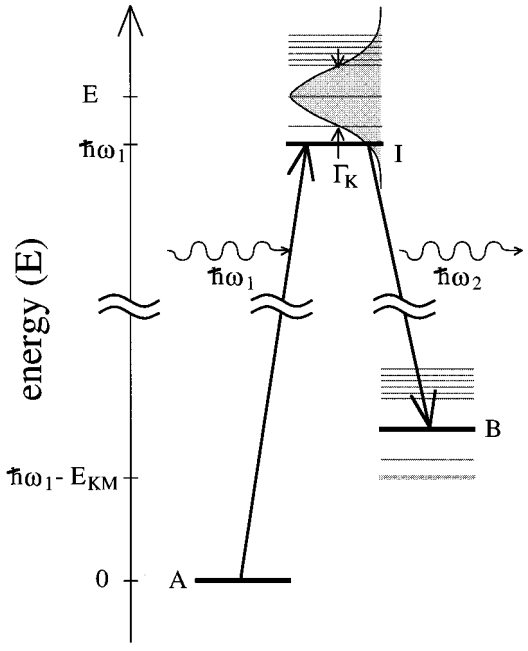

FIG. 8. A total energy diagram is shown for the absorption and emission processes, taking place through an intermediate state of nominal energy E. Here the incident energy $\hbar\omega_1$ is below E, but transitions take place because of the uncertainty in E, characterized by Γ_K. The transition probability to this particular intermediate state is proportional to $L_K(E-\hbar\omega_1)\cdot\mu^*(E)$. The intermediate state is assumed to fix the final state: thus the x-ray emission spectrum given in Eq. (4) directly reflects the intermediate-state distribution.

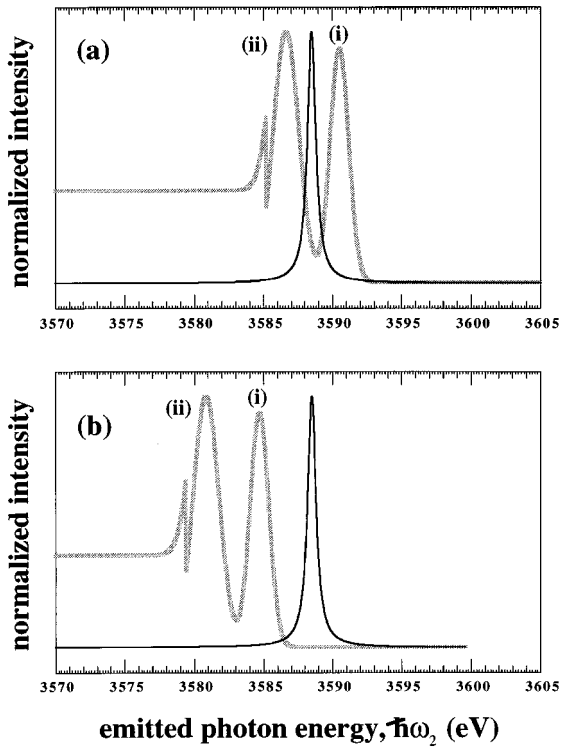

FIG. 9. The components of the potassium-K-emission construction based on Eq. (4) are plotted vs $\hbar\omega_2$: $L_K(\hbar\omega_2-E_{KM})$ and $\mu^*(\hbar\omega_1-\hbar\omega_2+E_{KM})$. For μ^*, the intermediate-state-lifetime broadening and beamline-monochromator-instrumental broadening have been stripped from the model fit to the absorption spectrum shown in Fig. 1(b). In (a), the construction of the potassium K_β emission spectrum for $\hbar\omega_1=3612.9$ eV [Fig. 2 (C)] is plotted. In (b), the construction of the potassium K_β emission spectrum for $\hbar\omega_1=3607.1$ eV [Fig. 2 (I)] is plotted.

tion establishes the emission spectrum: shifting this distribution to the diagram fluorescence energy as in Eq. (4) yields a predicted emission spectrum. Equation (4) omits the final-state lifetime and instrumental broadenings of the beamline monochromator and emission spectrometer.[12,20,27] It also omits the bandwidth of the shallow M states due to solid-state effects. However, as discussed below, Eq. (4) allows a simple interpretation of the energy shifts and line-shape variations in the threshold emission spectra.

Based on Eq. (4), we *constructed* emission spectra using the measured absorption spectra in Figs. 1 and 5. The main components of this construction for potassium K_β emission are plotted in Fig. 9. In order to convert the measured absorption spectra to μ^*, the K-hole lifetime[28] and beamline-monochromator broadening must be removed. Unfortunately, various deconvolution routines yielded unacceptable noise amplification. We instead fit the absorption spectra with the simplest model functions that captured their essential features, and from these curves the broadenings were directly removed. The fit to the potassium K absorption spectrum of Fig. 1 consists of two Lorentzian and Gaussian-broadened peaks and a broadened step function. The fit to the chlorine K absorption spectrum of Fig. 5 consists of three peaks[29] and a step function. We plot $\mu^*(\hbar\omega_1-\hbar\omega_2+E_{KM})$ versus $\hbar\omega_2$, using $E_{KM}=3588.5$ eV for potassium and $E_{KM}=2814.7$ eV for chlorine. $\mu^*(\hbar\omega_1-\hbar\omega_2+E_{KM})$ shifts

for different incident energies $\hbar\omega_1$. It is important to note that the peak energies of $\mu^*(\hbar\omega_1-\hbar\omega_2+E_{KM})$ are at exactly the $\hbar\omega_2$ values given by Eq. (1).

Figures 2 and 6 compare measured and constructed emission spectra. Beamline-monochromator and emission-spectrometer instrumental broadenings and the solid-state M bandwidth, as determined from the post-threshold fluorescence spectra, have been incorporated in the construction[27] to allow a more complete comparison. The final-state lifetime broadening is assumed negligible.[30] Previous constructions for Ar K_α emission yielded quantitative agreement with the measured emission spectra.[17] In the present work the constructed spectra qualitatively match the energy shifts and line shape changes of the measured spectra. The intensity of the constructed spectra follows that of the data fairly well over variations amounting to a factor of 20.

We see in the subthreshold resonant Raman spectra of Figs. 2 and 6 an energy offset between the data and the constructed spectra.[31] This discrepancy may stem from a failure in the ε-independent emission assumption that underlies the construction. In particular, binding-energy differences, i.e., differences in ε, between an intermediate-state core exciton and a final-state valence exciton would yield additional energy shifts in the emission spectra.[24] For both potassium and chlorine, the main peak in the data lies roughly half an eV below the corresponding feature in the construction; this peak in the resonant Raman regime is unambiguously associated with feature (i) in the absorption spectrum. Thus, the offset suggests that absorption feature (i) in the potassium and chlorine K absorption spectra are excitonic in origin. We note, however, that Sugiura and Sasaki[8] have combined fluorescence, absorption, and photoemission data to claim that in the potassium absorption the threshold for continuum transitions lies below feature (i). In general, direct comparison of core and valence exciton binding energies is not possible: the position of the continuum threshold in the core absorption is not a well-established quantity. Valence exciton binding energies can be estimated from the optical absorption of Teegarden and Baldini[32] and the electron energy loss spectroscopy of Creuzburg[33] to be roughly 1 and 3 eV.

In Figs. 2 (F) and 6 (F), $\hbar\omega_1$ is at the onset of strong absorption, and the emission spectra exhibit the asymmetry characteristic of this excitation regime, with a broader tail toward low $\hbar\omega_2$.[10] From Eq. (4), we attribute this asymmetry to the abrupt decline of $\mu^*(\hbar\omega_1-\hbar\omega_2+E_{KM})$ to high $\hbar\omega_2$ versus the more gradual K-hole-broadened tail of $L_K(\hbar\omega_2-E_{KM})$ to low $\hbar\omega_2$. The construction based on Eq. (4) also offers insight for $\hbar\omega_1$ values within the main absorption profile. Figure 9(a) is a plot of the construction for potassium emission at $\hbar\omega_1=3612.9$ eV: the two components are multiplied to yield the constructed spectrum of Fig. 2 (C). The origin of the broadening in the measured spectrum is clarified by the construction. An $\hbar\omega_1$ of 3612.9 eV centers the intermediate-state excitation distribution $L_K(E-\hbar\omega_1)$ between the two excitation features, (i) and (ii), of $\mu^*(E)$; thus there is a bimodal intermediate-state distribution, and this is reflected in the emission spectrum.

V. SUMMARY

Figures 2 and 6 demonstrate K_β resonant Raman emission spectra and their evolution into fluorescence at the potassium and chlorine K absorption thresholds. Absorption spectra of KCl have two distinct peaks at both the potassium and chlorine K thresholds, and these features are directly reflected in the resonant Raman spectra. Details of the line shape and its evolution are evaluated by multiplication of the Lorentzian-broadened excitation function with the excitation cross section, as derived from the absorption spectrum. Certain energy offsets between the data and this construction suggest that the associated intermediate states are excitonic in nature. Overall, however, the construction yields good agreement with the measured emission spectra, and the simple formulation allows a direct interpretation of energy, line shape, and intensity variations.

[1] J. W. Trischka, Phys. Rev. **67**, 318 (1945).

[2] L. G. Parratt and E. L. Jossem, Phys. Rev. **97**, 916 (1955).

[3] R. D. Deslattes, Phys. Rev. **133**, A390 (1964); **133**, A399 (1964).

[4] I. N. Mazalov, É. E. Vainshtein, and V. G. Zyryanov, Dokl. Akad. Nauk SSSR **164**, 545 (1965) [Sov. Phys. Dokl. **10**, 857 (1966)].

[5] S. T. Pantelides, Phys. Rev. B **11**, 2391 (1975).

[6] I. I. Gegusin, V. N. Datsyuk, A. A. Novakovich, L. A. Bugaev, and R. V. Vendrinskii, Phys. Status Solidi B **134**, 641 (1986).

[7] P. L. Cowan, Phys. Scr. **T31**, 112 (1989).

[8] C. Sugiura and H. Sasaki, Jpn. J. Appl. Phys. **32**, 1135 (1993).

[9] C. J. Sparks, Phys. Rev. Lett. **33**, 262 (1974).

[10] P. Eisenberger, P. M. Platzman, and H. Winick, Phys. Rev. Lett. **36**, 623 (1976); Phys. Rev. B **13**, 2377 (1976).

[11] A. F. Kodre and S. M. Shafroth, Phys. Rev. A **19**, 675 (1979).

[12] P. Suortti, Phys. Status Solidi B **91**, 657 (1979); S. Manninen, P. Suortti, M. J. Cooper, J. Chomilier, and G. Loupias, Phys. Rev. B **34**, 8351 (1986); K. Hämäläinen, S. Manninen, P. Suortti, S. P. Collins, M. J. Cooper, and D. Laundy, J. Phys. Condens. Matter **1**, 5955 (1989); K. Hämäläinen, S. Manninen, S. P. Collins, and M. J. Cooper, *ibid.* **2**, 5619 (1990).

[13] D. Schaupp, H. Czerwinski, F. Smend, R. Wenkus, M. Schumacher, A. H. Millhouse, and H. Schenk-Strauss, Z. Phys. A **319**, 1 (1984); H. Czerwinski, F. Smend, D. Schaupp, M. Schumacher, A. H. Millhouse, and H. Schenk-Strauss, *ibid.* **322**, 183 (1985).

[14] J. P. Briand, D. Girard, V. O. Kostroun, P. Chevalier, K. Wohrer, and J. P. Mossé, Phys. Rev. Lett. **46**, 1625 (1981).

[15] Y. Udagawa and K. Tohji, Chem. Phys. Lett. **148**, 101 (1988).

[16] G. E. Ice, E. Isaacs, and P. Zschack, Phys. Rev. B **47**, 6241 (1993).

[17] P. L. Cowan, in *Resonant Anomalous X-Ray Scattering*, edited by G. Materlik, C. J. Sparks, and K. Fischer (North-Holland, Amsterdam, 1994), p. 449.

[18] S. H. Southworth, Nucl. Instrum. Methods Phys. Res. B **87**, 247 (1994).

[19] M. A. MacDonald, S. H. Southworth, J. C. Levin, A. Henins, R. D. Deslattes, T. LeBrun, Y. Azuma, P. L. Cowan, and B. A. Karlin, Phys. Rev. A **51**, 3598 (1995).

[20] J. Tulkki and T. Åberg, J. Phys. B **13**, 3341 (1980); **15**, L435 (1982); J. Tulkki, Phys. Rev. A **27**, 3375 (1983); T. Åberg and J. Tulkki, in *Atomic Inner-Shell Physics*, edited by B. Crasemann (Plenum, New York, 1985), p. 419.

[21] T. Åberg and B. Crasemann, in *Resonant Anomalous X-Ray Scattering* (Ref. 17), p. 431.

[22] Y. Ma, N. Wassdahl, P. Skytt, J. Guo, J. Nordgren, P. D. Johnson, J. E. Rubensson, T. Boske, W. Eberhardt, and S. Kevan, Phys. Rev. Lett. **69**, 2598 (1992).

[23] Y. Ma, K. E. Miyano, P. L. Cowan, Y. Aglitzkiy, and B. A. Karlin, Phys. Rev. Lett. **74**, 478 (1995).

[24] W. L. O'Brien, J. Jia, Q.-Y. Dong, T. A. Callcott, K. E. Miyano, D. L. Ederer, D. R. Mueller, and C.-C. Kao, Phys. Rev. Lett. **70**, 238 (1993).

[25] P. L. Cowan, S. Brennan, R. D. Deslattes, A. Henins, T. Jach, and E. G. Kessler, Nucl. Instrum. Methods. Phys. Res. A **246**, 154 (1986).

[26] S. Brennan, P. L. Cowan, R. D. Deslattes, A. Henins, D. W. Lindle, and B. A. Karlin, Rev. Sci. Instrum. **60**, 2243 (1989).

[27] G. B. Armen and H. Wang, Phys. Rev. A **51**, 1241 (1995).

[28] Γ_K was taken to be 0.73 eV for potassium (Ref. 2) and 0.64 eV for chlorine [M. O. Krause and J. H. Oliver, J. Phys. Chem. Ref. Data **8**, 329 (1979)].

[29] The latter two chlorine K peaks were lumped together in plotting Eq. (1) for Fig. 7 because separate corresponding features could not reliably be resolved in the chlorine emission data.

[30] L. I. Yin, I. Adler, T. Tsang, M. H. Chen, D. A. Ringer, and B. Crasemann, Phys. Rev. A **9**, 1070 (1970).

[31] On the other hand, no clear offset is seen in Figs. 4 and 7 between the main peak energy positions and the energies predicted by the simple conservation formula of Eq. (1). The offset only appears when the more detailed calculation takes into account the energy widths of the excitation features.

[32] K. Teegarden and G. Baldini, Phys. Rev. **155**, 896 (1967).

[33] M. Creuzburg, Z. Phys. **196**, 433 (1966).